ELSEVIER

Materials Science and Engineering B76 (2000) 139–144

MATERIALS SCIENCE & ENGINEERING B

www.elsevier.com/locate/mseb

Characterization of semiconductor heterostructures by acousto-optical perturbation technique

I.V. Ostrovskii [a], O.A. Korotchenkov [a,*], R.M. Burbelo [a], H.G. Walther [b]

[a] *Taras Shevchenko Kiev University, Physics Faculty, Glushkova Avenue 6, 03680, Kiev 252022, Ukraine*
[b] *Friedrich Schiller University, Institute for Optics and Quantum Electronics, Jena 07743, Germany*

Received 10 November 1998; accepted 14 February 2000

Abstract

A new technique is developed for investigating defects at substrate/layer semiconductor interface. Acoustic waves (AW) are used to induce changes in the spectral dependence of the optical reflectance and transmission of semiconductor heterostructures together with photoacoustic (PA) and photoelectric (PE) imagings of the layers. The method is illustrated with experiments performed on n-type doped GaAs MBE layers of different quality (unintentionally doping and Si or Te controlled doping). The spectral peaks observed at about 37 and 29 meV inside the band gap are attributed to energy levels of Si and Te impurities, respectively. Two peaks ranged from 54 to 67 and 80–90 meV below the band gap in different samples are suggested to be due to two energy levels of As-vacancy related defects localized at the interface and influenced by electric fields and mechanical stresses in the boundary region. The exact energy position of these peaks is interpreted to be indicative of the interface quality. PA and PE imagings are employed to qualitatively determine electric charge conditions of the interface. It is demonstrated that the nonuniformity of the PE image increases for lower quality substrate/layer interface. Direct evidence is found that relates the interface charge to the spectral peak position of the As-vacancy related defect in acoustically perturbed reflectance spectra.

Keywords: Heterostructures; Interfaces; Acoustic waves; Optical spectra; Imaging

1. Introduction

Countless investigations have been performed on low-dimensional semiconductor structures, heterojunctions and superlattices, and their applications in electronic device [1–3]. These structures and devices have been studied by different spectroscopy methods such as luminescence, absorption, photocurrent spectroscopy, Raman scattering, etc. In particular, modulation spectroscopy techniques have often been used for studying optical critical-point structures and deformation potential parameters. Electro-, thermo- and piezo-modulation of absorption and reflectance spectra have commonly been employed in experiments [4–10]. Very recently, a new modulation technique utilizing electric fields of surface acoustic waves (AW) was reported [11]. This field perturbs the optical reflectivity of a semiconductor surface adjacent to the piezoelectric substrate, which drive surface AW, allowing derivative reflectance spectra to be obtained in a manner analogous to the photo-modulation technique.

Although, lattice imperfections such as point defects and dislocations localized in the interface and associated electric charges play a key role in device performance a reliable identification of interface local states is still lacking. It is well documented to the date that vibrational excitations of heterostructures can be localized in the vicinity of an interface [12,13]. Therefore, one might expect that plate AW transmitting through a substrate/layer sample could lead to disturbances in the interface with respect to its electric charges and strain parameters which are specific of the interface quality. By using optical spectroscopy techniques these disturbances can be detected thus providing a realistic opportunity to probe interface quality.

This work aims to present a technique developed for detecting the substrate/epitaxial layer defects and char-

* Corresponding author.
E-mail address: olegk@mail.univ.kiev.ua (O.A. Korotchenkov)

0921-5107/00/$ - see front matter
PII: S0921-5107(00)00429-3

acterizing electric charge conditions of the interface. The method is illustrated with GaAs heterostructures, which are widely employed in modern semiconductor technologies. The measurements of the optical reflectance and transmission of semiconductor heterostructures perturbed by AW are reported together with photoacoustic (PA) and photoelectric (PE) imaging of the layers.

2. Experimental

Experimental arrangements are exhibited in Fig. 1. Epitaxial layers of GaAs (1 in Fig. 1), unintentionally doped, and Si- and Te-doped, were used in experiments. The layers were grown by MBE on (100) GaAs wafers 2. Three groups of heterostructures, namely the sample of series # 1, 2 and 3 were obtained from three different laboratories. The thickness of the layer 1 ranged from 2.5 to 9 μm while the thickness of the wafer 2 was typically a few hundred microns. Electron concentrations in the layers at 300 K were found to be from 2.6×10^{15} to 5×10^{16} cm^{-3}.

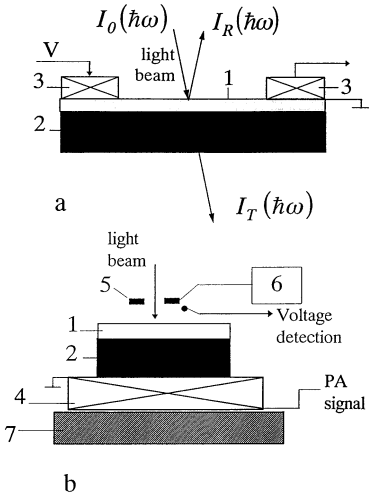

Fig. 1. Schematic drawing of experimental setups. (1) GaAs substrate, (2) GaAs layer, (3), (4) piezoelectric transducers, (5) capacitance electrode, (6) alignment system, (7) movable $X-Y$ stage.

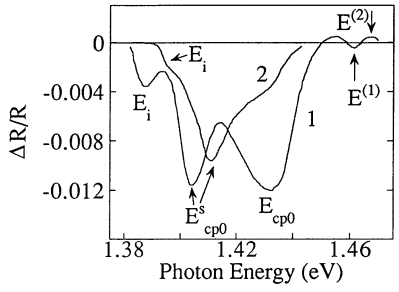

Fig. 2. Spectra of acoustically perturbed reflectance in Si-doped (series # 2 sample) (1) and Te-doped (series # 1 sample) (2) GaAs layers. $V = 13$ V, $f = 2.56$ (1) and 2.014 MHz (2).

AW were launched by placing zirconate–titanate piezoelectric transducers [3 in Fig. 1(a)] on the sample surface. One of the transducers drive the waves and the other one served as a detector of plate waves. Application of the rf voltage V to the exciting transducer generated Lamb waves in the plate with two orthogonal components of mechanical displacements that were parallel and perpendicular to the sample surface. It is worth noting that AW produces essentially nonuniform stress fields as opposed to the largest possible uniform distribution of stresses usually achieved with piezomodulation techniques [14]. The frequency f of AW ranged from 2 to 8 MHz. The AW intensity varied between 0.1 and 4.5 W cm^{-2} and was adjusted by changing the voltage V.

By measuring reflected (I_R) and transmitted (I_T) light intensities, the change of optical reflectance and transmission caused by AW was detected using a setup shown in Fig. 1(a). The change of the reflectance R was taken in this work not at the frequency f, as it does in traditional modulation techniques, but in terms of

$$\frac{\Delta R}{R} = \left[\frac{R(V) - R(0)}{R(0)}\right], \quad (1)$$

where $R(V)$ and $R(0)$ are the values of the reflectance taken at applied voltages V and $V = 0$, respectively. In the optical transmission measurements, the data were displayed in terms of $T = (I_T/I_0)$ shown in Fig. 1(a).

To detect spatially resolved PE signals, the sample was placed on a movable $X-Y$ stage 7 [Fig. 1(b)] equipped with a stepping motor drive. The minimum scanning step of the drive was roughly 10 μm. A modulated 488 nm light beam from an Ar^+ laser was focused onto the sample surface with a spot of 10 μm in diameter. A ring-shaped capacitance electrode 5 was mounted close to the sample surface in order to detect a photovoltage signal. Simultaneously, the PA signal was picked up by a disk-shaped piezoceramic transducer 4. Signal measurements, data processing and scanning control were provided by a PC. Images were plotted in a half-tone mode with ten gray levels. All measurements were performed at room temperature.

3. Results and discussion

Fig. 2 shows the spectral dependencies of $\Delta R/R$ taken in two samples at energies close to the band gap of GaAs. The peaks at $E_{cp0} = 1.426$ eV in spectra 1 and 2 correspond to electronic transitions between the valence band and the conduction band of GaAs. The appearance of these peaks is most likely related to electric fields imposed by AW, which perturb the optical reflectivity of the sample as already pointed out [11]. The validity of this explanation is confirmed by the occurrence of oscillating structure in spectrum 1

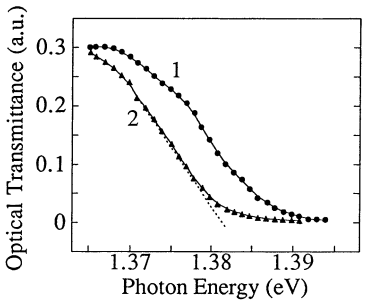

Fig. 3. Change of optical transmission edge due to acoustic perturbation of GaAs, Te layer (series # 1 sample). $V = 0$ (1) and 20 V (2), $f = 2.01$ MHz (1). Dashed line is a fitting line used to determine the edge slope.

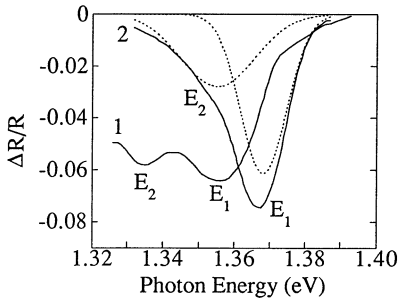

Fig. 4. Spectra of acoustically perturbed reflectance in GaAs (series # 3 sample) (1) and GaAs:Si (series # 2 sample) (2). $V = 6$ (1) and 13 V (2), $f = 7.32$ (1) and 2.56 MHz (2). Dashed lines show fitting of spectrum 2 to two Gaussian shapes.

marked by $E^{(1)}$ and $E^{(2)}$ which is usually observed in electro-modulation or photo-modulation techniques (see, [15]). It is worth noting that the strength of the oscillations was found to be sample series dependent. Thus, we failed to observe such oscillations in the series samples # 1 but they were detected in the series # 2 and # 3 samples.

The observed changes of the optical reflectance are accompanied by a low-energy shift of the optical transmission edge, as illustrated in Fig. 3. Similar shifts have previously been reported in various semiconductors and interpreted in terms of electric and stress fields accompanying acoustic wave disturbances [16–18].

Within the electric field approach, the shift of the fundamental optical absorption edge can be described in analogy with the Franz–Keldysh effect in externally applied electric fields. Thus, the strength F of the electric field pervading the series # 2 sample can be estimated from the energy position $E^{(m)}$ of the mth extremum in spectrum 1 of Fig. 2 [19]

$$E^{(m)} = E_0 + \Theta X(m), \quad (m = 1,2,\ldots) \tag{2}$$

where E is the photon energy, $\Theta = (e^2F^2\hbar^2/8\mu)^{1/3}$ is the characteristic energy, μ is the reduced interband effective mass, and $X(m) = [3(m - 1/2)/2]^{2/3}$. Using energies $E^{(1)}$ and $E^{(2)}$ of the first and second extrema in Fig. 2, respectively, and taking $\mu = 0.06\ m_0$ in GaAs [20,21], we find $F \approx 2.7 \times 10^4$ V cm^{-1}. Such field strength appears to be capable of producing the shift of the transmission edge exhibited in Fig. 3, as will be demonstrated below. We, therefore, conclude that the description of the data of Figs. 2 and 3 in the context of electric fields imposed by AW remains to be a reasonable assumption. However, it should be noted that the strength of the oscillations seen in Fig. 2 is relatively low as opposed to the fine structure with at least four extrema usually observed in electro-modulation techniques [4–10]. Hence, the reported values of F should be taken to be a rough estimate of electric fields strengths inside the samples.

On the low-energy side of the E_{cp0} peak, additional spectral features labeled by E^s_{cp0} are seen in spectra of Fig. 2. The E^s_{cp0} peak energy decreases with increasing the AW amplitude such that the separation ($E^s_{cp0} - E_{cp0}$) amounts to ≈ 25 meV at the maximum driving amplitudes. The E^s_{cp0} peaks are believed to arise from the tailing of the absorption edge into the energy gap due to acoustic perturbation, and from the small splitting of the valence band in acoustic strain fields. Detailed study of the E_{cp0} and E^s_{cp0} peaks in the spectra exhibited in Fig. 2, published elsewhere.

We will now discuss the peaks E_i in Fig. 2, which are located further below the energy gap. It has previously been reported that peaks shifted ≈ 35–40 meV below the gap are often obtained in the spectra of electro- and photo-reflectance of GaAs (see [4] and references therein). They are believed to arise from the shallow impurity levels, particularly from those of Si. Therefore, we are attempting to assign the E_i peaks to impurity levels. It is naturally to attribute the E_i peak in the spectrum of the Te-doped layer (spectrum 2 in Fig. 2) to Te impurities while that in the spectrum of the Si-doped layer (spectrum 1 in Fig. 2) to Si impurities. With that in mind, the energy positions of appropriate levels have been determined by decomposing spectra 1 and 2 of Fig. 2 into three Gaussian shapes which correspond to the E_{cp0}, E^s_{cp0} and E_i peaks. Estimated depth of the energy levels of Si and Te impurities are about 37 and 29 meV inside the band gap, respectively. As far as we are aware, the depth of ≈ 29 meV for the energy level of Te impurities is reported for the first time.

Fig. 4 represents the spectra of $\Delta R/R$ for deeper band gap defect states. Two spectral features denoted by E_1 and E_2 have been observed in all investigated samples. The E_2 peak appears as a shoulder in spectrum 2 so that it has been resolved by decomposing the line shape into two Gaussians, as shown by the dashed curves in Fig. 4. Interestingly, the energy position of these peaks has been found to be nearly the same for the samples of the same series although it has varied substantially with the sample series, i.e. with the fabrication process as spectra 1 and 2 in Fig. 4 illustrated.

Thus, the E_1 peaks can be attributed to levels with energy depths of 67 and 54 meV, respectively, for spectra 1 and 2 in Fig. 4. Levels with the depths of about 90 and 80 meV correspond to the E_2 peaks in spectra 1 and 2, respectively.

Accounting for their energy positions, the E_1 and E_2 peaks are likely to originate from arsenic vacancies V_{As}. Indeed, both the E_1 and E_2 peaks have been found to similar shift from sample to sample thus suggesting that both of them be due to the same center. It is also worth nothing that so-called $E1$ levels with the depth of 45 meV have previously been observed [22] and they have been attributed to V_{As}. Further, positron-lifetime spectroscopy experiments have revealed two ionization levels at $E_c - 30$ meV ascribed to the transition $V^-_{As} \rightarrow V^0_{As}$ and at $E_c - 140$ meV attributed to the transition $V^0_{As} \rightarrow V^+_{As}$ [23]. The values of the energy depths for two levels of V_{As} obtained in our studies slightly diverges from those reported in [22,23]. However, it should be emphasized that Saarinen and coworkers [23] did not establish whether the As vacancies are isolated or are part of defect complexes.

It is therefore reasonable to assume that both the E_1 and E_2 peaks exhibited in Fig. 4 correspond to V_{As} in different charge states. The dependence of the energy position of these peaks on the fabrication process (spectra 1 and 2 in Fig. 4) implies that the detected defects at least partly are localized in the interface. Assuming this to be the case, electric fields and mechanical stresses in the vicinity of the interface likely shift the defect energy

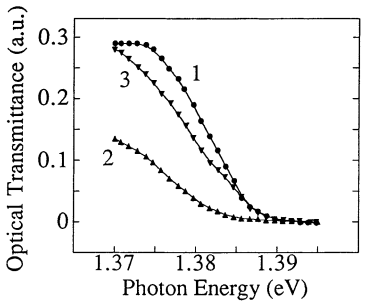

Fig. 5. Change of optical transmission edge due to acoustic perturbation of GaAs layer (series # 3 sample). $V = 0$ (1), 20 V (2) and after AW removal (3), $f = 2.21$ MHz (1).

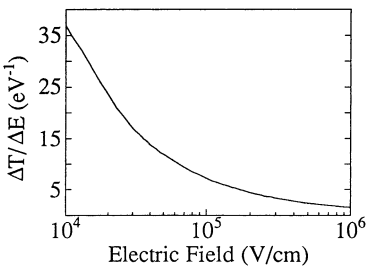

Fig. 6. Change of the transmission edge slope with the electric field strength. See text for details.

levels to lower energy compared to those in a bulk. Therefore, the amount of the low-energy shift of the E_1 and E_2 peaks compared to the bulk value is directly related to the quality of epitaxial layers.

In order to justify the conclusion made, acoustically disturbed optical transmission spectra have been compared with the PA and PE images of the layers. For this purpose, two of the samples of series # 1 and # 3 with markedly different positions of the E_1 and E_2 peaks in the spectra of $\Delta R/R$ have been chosen for further experiments. Strikingly different behaviors of acoustically disturbed optical transmission spectra are observed in these samples. First, almost no change of the transmission edge slope is seen in the series # 1 sample (spectra 1 and 2 in Fig. 3) whereas the series # 3 sample exhibits a remarkable change of the edge slope in acoustic perturbing fields (spectra 1 and 2 in Fig. 5). Moreover, while the low-energy shift of the transmission edge seen in Fig. 3 completely disappeared, to within an experimental error, after removal of the perturbation (not shown in Fig. 3) the change of the edge slope exhibited in Fig. 5 persists well after AW removal (spectra 1 and 3 in Fig. 5). A complete recovery of the initial transmission spectrum in the series # 3 sample (i.e. spectrum 1 in Fig. 5) has been achieved in some days after removing the perturbation.

Taking into account that both the low-energy shift and the change of the transmission edge slope are known to accompany electric field effects in semiconductors (see, [20,21]), we hence suggest a remarkable change of electric fields inside the samples due to acoustic perturbation, as already pointed out. These changes are further assumed to be an interface-quality dependent as follows from the above consideration.

In the framework of Franz–Keldysh effect, optical absorption coefficient α below the band gap E_g is related to the externally applied electric field F as [24]

$$\alpha = A\left[\frac{\Theta^{3/2}}{(E_g - E)}\right]\exp\left\{\left(-\frac{4}{3}\right)\left[\frac{(E_g - E)}{\Theta^{3/2}}\right]\right\}, \quad (3)$$

where A is material constant. The transmission spectra $T(E)$ are then described by

$$T = (1 - R)^2\frac{\exp(-\alpha d)}{[1 - R^2\exp(-2\alpha d)]}, \quad (4)$$

where $R = (n-1)^2/(n+1)^2$, n is the refractive index, and d is the thickness of the sample. The transmission spectra have been computed and plotted for different electric field strengths F and from these the slope $\Delta T/\Delta E$ as a function of F has been obtained; see Fig. 6. Using the change of the edge slope from $\Delta T/\Delta E \approx 25$ eV^{-1} for spectrum 1 in Fig. 5 to $\Delta T/\Delta E \approx 10$ eV^{-1} for spectrum 2 in Fig. 5, appropriate change of electric field strengths can be obtained from Fig. 6. We find $F_1 \approx 2 \times 10^4$ V cm^{-1} (spectrum 1 in Fig. 5) and $F_2 \approx 6 \times 10^4$ V cm^{-1} (spectrum 2). Comparing spectra 1 and 3 in

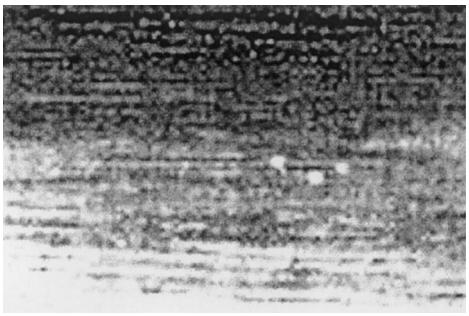

Fig. 7. PA images of GaAs layer (series # 3 Sample). The area is 2.40×1.88 mm^2.

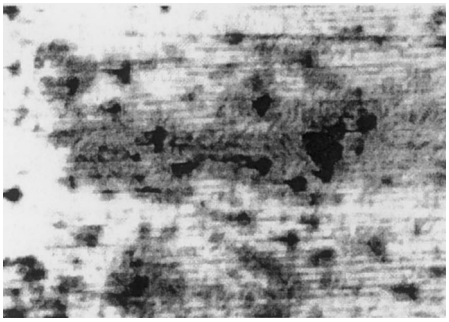

Fig. 8. PE image of GaAs layer (series # 3 sample). The area is 2.40×1.88 mm^2.

Fig. 5, we find the long-lived change of F imposed by AW to be $\approx 3 \times 10^4$ V cm^{-1} which is in excellent agreement with the value (2.7×10^4 V cm^{-1}) obtained from the $\Delta R/R$ oscillations shown in Fig. 2.

The presented evidence leads us to conclude that the acoustic perturbation modifies electric fields near the interface. It has been well documented that the optical reflectance at photon energies close to the band gap depends rather sensitively on the electric potential at the internal interface [25,26]. It is therefore understood that the change of the interface potential in acoustic perturbing fields is likely responsible for the spectral features in optical reflectance exhibited in Fig. 2 and for the low-energy shifts of transmission spectra seen in Figs. 3 and 5.

A far more striking observation is the correspondence between the E_1 and E_2 peak positions in spectra of Fig. 4 and the size of the perturbation effect on the transmission spectra shown in Figs. 3 and 5. The greater the influence of acoustic perturbation on the optical edge (spectra 1 and 2 in Fig. 5 compared to the ones in Fig. 3), the greater the low-energy shifts of the E_1 and E_2 peak positions are observed (spectra 1 and 2 in Fig. 4). Obviously, this is a crucial observation, which suggests that our technique is applicable for detecting interface defects and interface quality with respect to the charge condition of the interface.

To find unambiguous proof for this suggestion, PE and PA imagings of the layers have been performed. The PA technique is related to photothermal processes which accompany the conversion of absorbed light into heat and then into AW [27]. The PE studies with an ac signal arisen in semiconductors due to a modulated illumination with a laser light. This signal originates from two physical processes. First, extra carriers created by the laser beam modify the surface potential (band bending effect) due to a capture of charged carriers by the surface traps. The second process is related to the transfer of carriers of opposite charges into a space charge regions formed, e.g. by p–n junctions, clusters of charged defects, etc. In particular, observation of photoelectromotiveforce makes it possible to study near surface regions of the samples by scanning a focused light beam across the surface, that is by photoelectric microscopy techniques.

Typical PA and PE images taken from the same region of the series # 3 sample are shown in Figs. 7 and 8, respectively. One can conclude that the nonuniformity of the PE image is strikingly larger than that the PA image. To interpret this difference, one should keep in mind that the PA image reflects the thermal nonuniformities of the sample while the PE image appears to be due to the electric charge nonuniformities of the layer. Furthermore, the PA images are averaged over the depth of the thermal diffusion length, which is about 20 μm in GaAs at the employed modulation frequency of the laser light close to 80 kHz. In contrast, the PE images depend on the light penetration depth inside GaAs, which is roughly 1 μm for a 488 nm light. The actual penetration depth is a little bit greater because of the secondary emission inside the sample. With that in mind, the PA image in Fig. 7 is related to the thermal uniformity of the investigated region since the image appears to be almost homogenous. The relative decrease in the PA signal from the top to the bottom seen in Fig. 7 has been found to arise from the change of the spatial sensitivity of a piezoelectric receiver and is not related to the sample properties.

The PE image exhibited in Fig. 8 contains numerous dark dots as opposed to a nearly uniform PA image displayed in Fig. 7. The dots obviously reflect substantial changes of the electric potential across the imaged region. It is therefore most likely that numerous charge defects are revealed in the PE image. In this picture, the local built-in fields change the surface potential and thus form a photoelectromotiveforce signal due to capacitance between the sample surface and electrode 5 in Fig. 1(b). Taking into account the small light penetration depth, this verifies the existence of charged nonuniformities in the subsurface region with the depth of ~ 1 μm. We, therefore, suggest that the nonuniform PE image in Fig. 8 arise in the interface region of the series # 3 sample with a high defect concentration at the interface. It has been verified that both the PE and PA images of the series # 1 samples have been found to be

rather smooth and uniform, in accord with the above suggestion on the better interface quality in the series # 1 samples compared to that in the series # 3 samples.

4. Conclusions

An acousto-optical perturbation technique is developed for characterizing the quality of semiconductor heterostructures with respect to defects localized in the interface and interface charges. The technique employs the optical reflectance and transmission of the structures affected by AW together with the PA and PE imaging of the samples. Two levels ranged from 54 to 67 and 80–90 meV into the energy gap are attributed to two energy levels of As-vacancy related defects localized at the interface. It is shown that the energy position of these levels within the range is indicative of electric charge conditions at the interface. Comparing the PE and PA images of the samples proves the occurrence of electric charges at the interface such that the nonuniformity of the PE image increases for lower quality substrate/layer interface.

Acknowledgements

We acknowledge Bundesministerium für Bilding, Wissenschaft, Förschung und Technologie, Deutschland and ISSEP Program of International Soros Foundation for partial financial support.

References

[1] G. Bastard, J.A. Brum, R. Ferreira, in: H. Ehrenreich, D. Turnbull (Eds.), Solid State Physics, vol. 44, Academic Press, Boston, 1991, p. 229.
[2] F. Bechstedt, R. Enderlein, Semiconductor Surfaces and Interfaces, Academie-Verlag, Berlin, 1988.
[3] T. Ogawa, Y. Kanemitsu, Optical Properties of Low-Dimensional Materials, World Scientific, Singapore, 1995.
[4] M. Cardona, Modulation Spectroscopy, Academic Press, New York, 1969.
[5] H. Shen, J. Lumin. 62–63 (1994) 287.
[6] F.H. Pollak, H. Shen, Mater. Sci. Eng. R10 (1993) 275.
[7] W. Zhou, H. Shen, J. Pamulapati, P. Cooke, M. Dutta, Phys. Rev. B 51 (1995) 5461.
[8] F.H. Pollak, in: M. Balkanskii (Ed.), Handbook on Semiconductors, vol. 2, North-Holland, Amsterdam, 1994, p. 527.
[9] O.J. Glembocki, B.V. Shanabrook, in: D.G. Seiler, C.L. Littler (Eds.), Semiconductors and Semimetals, vol. 36, Academic Press, New York, 1992, p. 221.
[10] A.K. Ramdas, S. Rodriquez, in: D.G. Seiler, C.L. Littler (Eds.), Semiconductors and Semimetals, vol. 36, Academic Press, New York, 1992, p. 137.
[11] I.J. Fritz, T.M. Brennan, Semicond. Sci. Technol. 12 (1997) 19.
[12] R. Hessmer, T. Huber, T. Egeler, M. Haines, G. Tränkle, G. Weimann, G. Abstreiter, Phys. Rev. B 46 (1992) 4071.
[13] A. Mlayah, R. Grac, G. Armelles, R. Carles, A. Zwick, F. Briones, Phys. Rev. Lett. 78 (1997) 4119.
[14] A. Gavini, M. Cardona, Phys. Rev. B 1 (1970) 672.
[15] B.O. Seraphin, N. Bottka, Phys. Rev. 139 (1965) A560.
[16] I.V. Ostrovskii, JETP Lett. 34 (1981) 446.
[17] I.V. Ostrovskii, O.A. Korotchenkov, Solid State Commun. 82 (1992) 267.
[18] I.V. Ostrovskii, Acoustoluminescence and Crystal Defects (in Russian), Vyshcha Shkola, Kiev, 1993.
[19] D.E. Aspnes, A.A. Studna, Phys. Rev. B 7 (1973) 4605.
[20] J.I. Pankove, Optical Processes in Semiconductors, Dover, New York, 1975.
[21] K. Seeger, Semiconductor Physics, Springer, Berlin, 1997.
[22] A. Jorio, C. Rejeb, M. Pareteau, C. Carlone, S.M. Khanna, J. Appl. Phys. 74 (1993) 2310.
[23] K. Saarinen, P. Hautojärvi, P. Lanki, C. Corbel, Phys. Rev. B 44 (1991) 10585.
[24] J. Callaway, Phys. Rev. 130 (1963) 549.
[25] B.O. Seraphin, R.B. Hess, N. Bottka, J. Appl. Phys. 36 (1965) 2242.
[26] B.O. Seraphin, R.B. Hess, Phys. Rev. Lett. 14 (1965) 138.
[27] A. Rosencwaig, Photoacoustics and Photoacoustic Spectroscopy, Wiley, New York, 1980.